IAHR AIRH

25th IAHR International Symposium on Ice
Trondheim, June 14 to 18, 2020

Elastic moduli of sea ice and lake ice calculated from in-situ and laboratory experiments

A. Marchenko[1], J. Grue[2], E. Karulin[3], R. Frederking[4], B. Lishman[5], P. Chistyakov[6], M. Karulina[3], D. Sodhi[7], C. Renshaw[8], A. Sakharov[6], V. Markov[6], E. Morozov[9], M. Shortt[10], J. Brown[11], A. Sliusarenko[12], D. Frey[9]

[1]*The University Centre in Svalbard*
PO Box 156, N-9171 Longyeabryen, Norway
Aleksey.Marchenko@unis.no
[2]*University of Oslo, Oslo, Norway*
[3]*Krylov State Research Centre, St.-Petersburg, Russia*
[4]*National Research Council Canada, Ottawa, Canada*
[5]*London South Bank University, London, UK*
[6]*Lomonosov Moscow State University, Moscow, Russia*
[7]*Cold Regions Research and Engineering Laboratory, USA*
[8]*Dartmouth College, Hannover, USA*
[9]*Shirshov Institute of Oceanology, Moscow, Russia*
[10]*London South Bank University, London, UK*
[11]*National Research Council Canada, St'-Johns, Canada*
[12]*Soft Engineering, Kiev, Ukrain*

The effective elastic modulus of ice is an important physical parameter for the calculation of ice stresses in different situations when ice deformations are small. In the present paper the review of methods used for the calculation of the elastic modulus of ice is performed, new tests for the calculation of the elastic modulus are described, and their results are discussed. Field experiments with floating vibrating ice beams with fixed ends were performed in March and November 2019 on sea ice of the Van Mijen Fjord and fresh-water ice of a lake near Longyearbyen. Laboratory experiments with vibrating cantilever beams were performed in the cold laboratory of UNIS in November 2019. The results are compared with the values of the effective elastic modulus obtained in quasi-static tests with floating cantilever beams, and with in-situ dynamic tests where the effective elastic modulus was measured by the speed of sound waves.

1. Introduction

Elastic moduli of ice are important characteristics used for the formulation of rheological models of ice. Measurements of elastic constants of ice crystal were performed by Jona and Scherrer (1952) using ultrasonic waves with frequencies of 15-18 MHz, and by Zarembovitch and Kahane (1964) using the same method with wave frequencies of 6-14 MHz. Green and Mackinnon (1956), Bogorodskii (1964) and Dantl (1969) used the direct ultrasonic pulse propagation method. Gammon et al (1980) and Gagnon et al (1988) detrmined the elastic constants of ice by Brillouin spectroscopy. It was discovered that elastic constant characterizing propagation of longitudinal waves increases with the temperature decrease and changes in the range from 9.8 GPa to above 13 GPa. Dantl (1969) determined the frequency dependence of elastic constant of ice in the range of 4-190 MHz and their dependence from the temperature from the melting point to -140 C.

Sinha (1989) derived the practical elastic moduli for polycrystalline ice using the data of Dantl (1969) and averaging procedure applied to a polycrystalline mass having randomly oriented grains (Voight, 1910). For the columnar-grained ice with horizontal and randomly oriented c-axes Sinha (1989) derived the formula describing temperature dependence of the longitudinal elastic modulus in the vertical and horizontal directions $E_v = E_{v,0} - c_v T$ and $E_h = E_{h,0} - c_h T$, where $E_{v,0} = 9.61$, $E_{h,0} = 9.39$ GPa, $c_v = 0.011$ GPa/C, $c_h = 0.013$ GPa/C, and T is the temperature (°C). According to formula (1) the vertical and horizontal elastic moduli increases respectively from 9.61 GPa to 9.72 GPa and from 9.39 GPa to 9.52 GPa when the ice temperature decreases from 0°C to -10°C. Dependencies of E_v and E_h from the temperature are shown in Fig. 1.

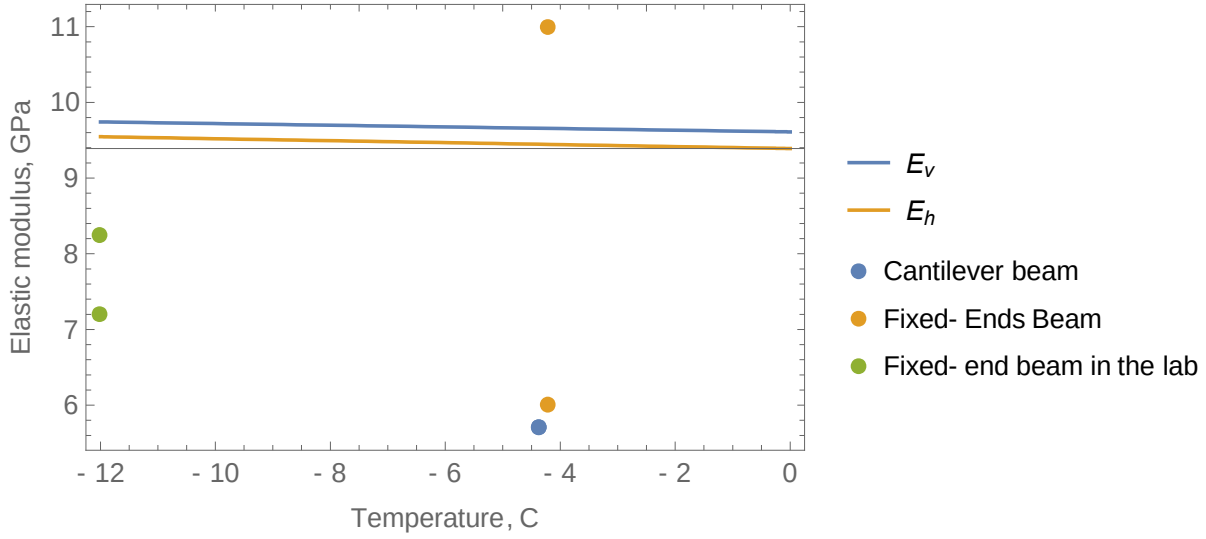

Figure 1. Elastic moduli of fresh ice versus the temperature.

Elastic modulus of sea ice was measured by Langleben and Pounder (1963) by seismic resonance experiments. Their data are approximated by the formula $E = 10 - 0.0351\,\nu_b$, where ν_b is the liquid brine content (ppt). Their measurements were performed for $0 < \nu_b < 90$ ppt. Slesarenko and Frolov (1972) measured elastic modulus of sea ice by the ultrasonic pulse method in the range $0 < \nu_b < 220$ ppt. Vaundrey (1977) calculated apparent elastic modulus from the results of laboratory and field tests on flexural strength. His empirical equation was included in ISO19906 as $E = 5.31 - 0.436\sqrt{\nu_b}$. Assur (1971) recommended

for practical use the formula $E = E_f(1 - 0.001\nu_b)^4$, where E_f is the elastic modulus for fresh ice assumed equal to 9.5 GPa. All above mentioned results are shown in Fig. 2.

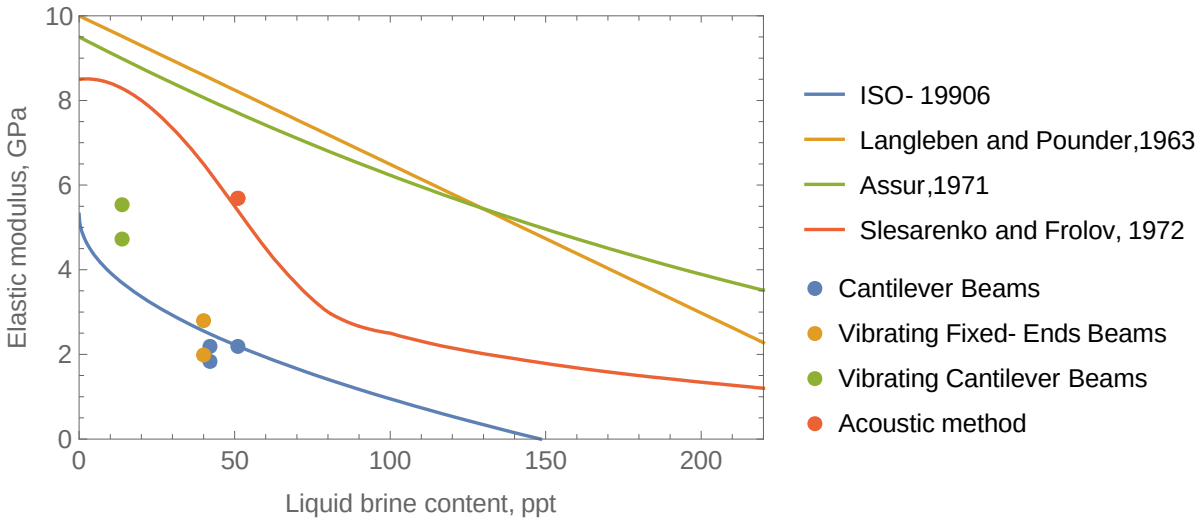

Figure 2. Elastic modulus of sea ice versus the liquid brine content.

In the present paper we perform the elastic modulus of fresh-water lake ice and sea ice calculated from the field tests with floating cantilever beams, floating fixed-ends beams, and laboratory tests with fixed end beams. All field tests were performed on sea ice in the Van Mijen fjord, and fresh ice in the lake near Longyearbyen in Spitsbergen. Laboratory tests were performed with ice beams sawn from sea ice in the places of the field works.

2. Tests with floating cantilever beams

Tests with floating cantilever beams (FCB tests) of sea ice were performed in the Vallunden lake (lagoon) near Svea in the Van Mijen fjord in March of 2019. Tests with floating cantilever beams of fresh ice were performed on the lake near Longyearbyen in November 2019. Figure 3 shows schematic of the test with downward bending of floating cantilever beam. Hydraulic equipment used in the tests is described in (Karulina et al., 2019). In 2019 measurements of vertical displacements was performed in several points located in the middle of the beam surface with LVDT displacement sensors (HBM). Data of the load cell and displacement sensors were collected by the amplifier SomatXR MX840B-R. Locations of the displacement measurements in the four tests are shown in Fig. 3c. The hydraulic cylinder and the displacement sensors were mounted on different metal frames R1 and R2 (Fig. 3b). The frames were fastened on the ice with ice screws. Figure 6 shows similar frame with the displacement sensors mounted near the beam with fixed ends. Further three tests (1,2,3) with sea ice beams and one test (4) with fresh ice beam are described.

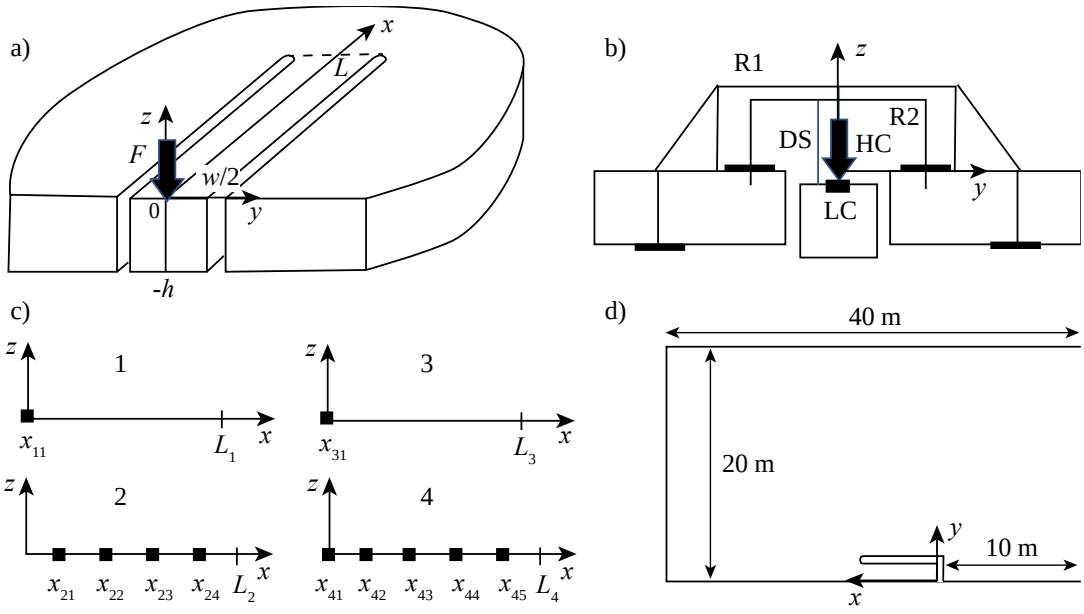

Figure 3. Schematic of the test with floating cantilever beam (FCB test) (a). Rig R1 is equipped with hydraulic cylinder (HC) and load cell (LC), rig R2 is equipped with displacement sensors (DS) (b). Locations of the measurements of vertical displacements at the beam axis in tests 1-4 (c). Dimensions of the computational domain (d).

Lengths and widths of the cantilever beams, ice thickness and locations of displacement sensors in the frame reference (x, y, z) shown in Fig. 3a are given below

$$\begin{aligned}
&1\text{: } L_1 = 3.4\ \text{m},\ w_1 = 0.7\ \text{m},\ h_1 = 0.72\ \text{m},\ x_{11} = 0.0\ \text{m};\\
&2\text{: } L_2 = 3.36\ \text{m},\ w_2 = 0.68\ \text{m},\ h_2 = 0.73\ \text{m},\ x_{21} = 0.67\ \text{m},\ x_{21} = 0.67\ \text{m},\\
&x_{22} = 1.28\ \text{m},\ x_{23} = 1.88\ \text{m},\ x_{24} = 2.44\ \text{m};\\
&3\text{: } L_3 = 3.94\ \text{m},\ w_3 = 0.74\ \text{m},\ h_3 = 0.75\ \text{m},\ x_{31} = 0.0\ \text{m};\\
&4\text{: } L_4 = 3.0\ \text{m},\ w_4 = 0.53\ \text{m},\ h_4 = 0.515\ \text{m},\ x_{41} = 0.0\ \text{m},\ x_{42} = 0.70\ \text{m},\\
&x_{43} = 1.30\ \text{m},\ x_{44} = 1.90\ \text{m},\ x_{45} = 2.48\ \text{m}.
\end{aligned} \quad [1]$$

The mean values of the ice temperatures and salinities measured during the tests near the beams are $T_1 = -6.14$ C, $S_1 = 4.93$ ppt, $T_2 = -6.11$ C, $S_2 = 4.93$ ppt, $T_3 = -5.86$ C, $S_3 = 5.74$ ppt, $T_4 = -4.39$ C, $S_4 = 0.0$ ppt. For the calculation of the elastic modulus numerical simulations were performed by the finite element method in the program COMSOL Multiphysics 5.4. The simulations are performed to model the beam deformations near the root (Karulin et al., 2019). Figure 3d shows the computational domain including a half of the cantilever beam. Symmetry boundary condition was used along the axis x and on the right boundary of the computational domain parallel to the axis y. Other boundaries on the plane (x, y) and the upper surface at $z = 0$ were free. At the ice bottom the elastic foundation imitating buoyancy force was used as a boundary condition. Sea density was equal to 920 kg/m3, and fresh ice density was set to 916 kg/m3. The Poisson's ratio was taken to be equal to 0.33. Linear elastic analysis was used for the modeling.

Measured forces were used directly in the simulations of each test. Elastic modulus was chosen by iteration to minimize the difference between calculated and measured displacements. Forces versus measured and computed displacements are shown in Fig. 4 for each of the tests. The values of adjusted elastic moduli are $E_1 = 2.2\text{GPa}, E_2 = 1.83\text{GPa}, E_3 = 2.2\text{GPa}, E_4 = 5.7\text{GPa}$.

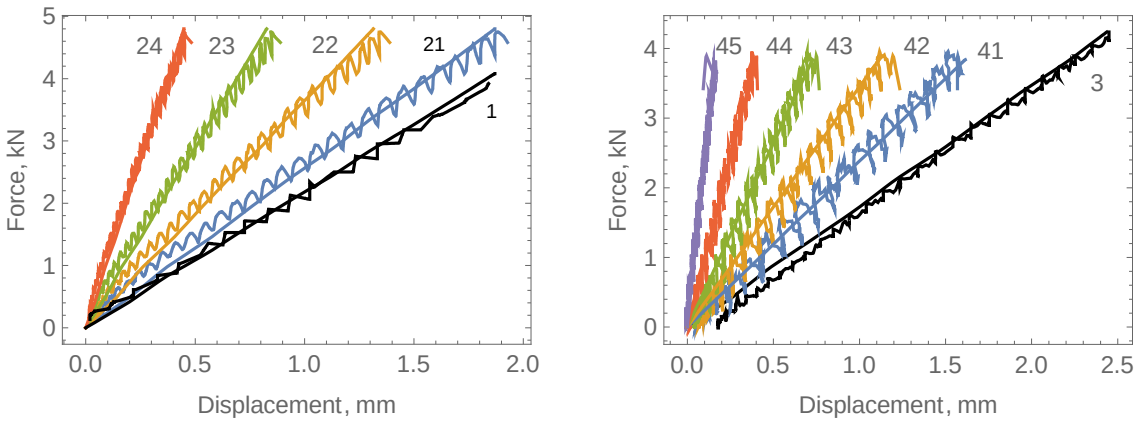

Figure 4. Forces versus displacements in tests 1-4. Solid straight lines correspond to the results of numerical simulations, curved lines correspond to the experimental data.

3. Tests with floating vibrating fixed-ends beams

Floating fixed-ends beam is shown in Fig. 5a. Natural frequencies of bending oscillations of the beam depend on the elastic modulus. In the test the beam oscillations are excited by a mechanic pulse and the beam motion is registered with accelerometers deployed on the beam surface. In the test on sea ice the beam was lifted in the middle by a chain connected to a winch, and then the chain was released by a release-hook (Fig. 6). This test is further named VFEB test. Two accelerometers are visible in the figure at the beam axis in the middle of the beam and to the left from the middle. In the test on fresh-water lake ice the pulse was applied by a jump of a person on the beam in the middle. Accelerometers Bruel & Kjær DeltaTron Type 8344 designed for the measurements of vibrations in the frequency range from 0.2 Hz to 3 kHz were used. The data of accelerometers were collected by the amplifier.

It is assumed that oscillations of an ice beam on hydraulic foundation are described by the equation

$$(\rho_i h + m_{ad})\frac{\partial^2 \eta}{\partial t^2} + \frac{Eh^3}{12}\frac{\partial^4 \eta}{\partial x^4} + \rho_w g \eta = 0, \qquad [2]$$

where η is the beam elevation, ρ_i and ρ_w are the ice and water densities, h is the ice thickness, m_{ad} is the added mass per unit area of the beam surface, E is the elastic modulus of ice, g is the gravitational acceleration, t and x are the time and the coordinate directed along the beam axis.

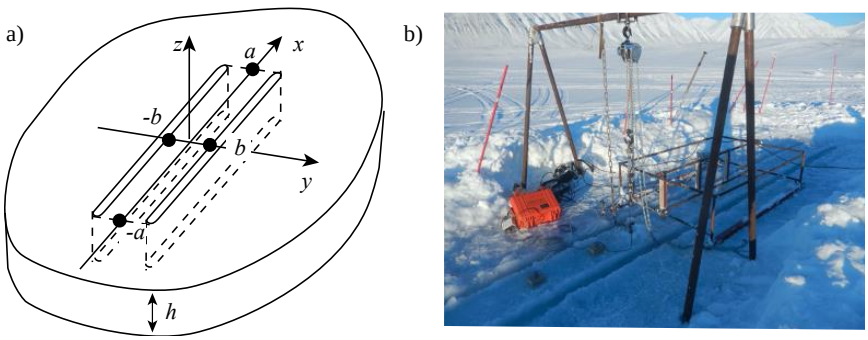

Figure 5. Schematic of the test with floating vibrating fixed-ends beam (VFEB test) (a). Photograph of in-situ VFEB test. Svea, March 2019 (b).

Boundary conditions for the fixed ends beam are

$$\eta = 0, \frac{\partial \eta}{\partial x} = 0, x = \pm a, \quad [3]$$

where $2a$ is the beam length. Periodical solution of [2] is expressed by formulas

$$\eta = e^{i\omega t} \sum_{j=1}^{4} C_j e^{ik_j x} + C.C., \quad [4]$$

where ω is the frequency, C_j are constants and k_j are the roots of the equation

$$\omega^2 - \omega_b^2 = \frac{Eh^3 k^4}{12(\rho_i h + m_{ad})}, \omega_b^2 = \frac{\rho_w g}{\rho_i h + m_{ad}}. \quad [5]$$

Here ω_b is the frequency of the natural oscillations of the floating ice due to the balance between the gravity and buoyancy forces.

The roots of equation (5) are determined by the formulas

$$k_{1,2} = \pm\alpha, k_{3,4} = \pm i\alpha, \alpha = \sqrt[4]{\frac{12(\omega^2 - \omega_b^2)(\rho_i h + m_{ad})}{Eh_i^3}}, \omega^2 > \omega_b^2, \quad [6]$$

$$k_{1,2} = \pm\alpha e^{i\pi/4}, k_{3,4} = \pm\alpha e^{-i\pi/4}, \alpha = \sqrt[4]{\frac{12|\omega^2 - \omega_b^2|(\rho_i h + m_{ad})}{Eh^3}}, \omega^2 < \omega_b^2, \quad [7]$$

Substituting formulas [4] and [6] or [4] and [7] in boundary conditions [3] we find a system of linear homogeneous equations for the calculation of constants C_j. The determinant of the system should be zero for the existence of nonzero solution. It is known that there is no nonzero solution in static case by $\omega = 0$. Therefore, nonzero solution is also absent in case $\omega^2 < \omega_b^2$, since the solution is expressed through the same eigen function as in the static case. Thus, the natural modes have frequencies greater ω_b.

The characteristic equation for symmetric mode by $\omega^2 < \omega_b^2$ has the form

$$\tan(\alpha a) + \tanh(\alpha a) = 0. \quad [8]$$

Since the first root is equal to $\alpha = 2.365/a$ then the first natural frequency is expressed by the formula

$$\omega_1 = \sqrt{\omega_b^2 + \frac{Eh^3}{12(\rho_i h + m_{ad})}\left(\frac{2.365}{a}\right)^4}. \quad [9]$$

The shape of the first mode is described by the equation

$$\eta/\eta_0 \approx 0.883\cos(2.365x/a) + 0.117\cosh(2.365x/a); \eta = \eta_0, x = 0. \quad [10]$$

Formula (9) could be used for the calculation of the elastic modulus E as follows

$$E = \frac{12(\omega_1^2 - \omega_b^2)(\rho_i h + m_{ad})}{h^3}\left(\frac{a}{2.365}\right)^4. \quad [11]$$

The added mass effect was estimated from the consideration of potential motion of the water in the region $z < -h$ (Fig. 4a). Normal water velocity at the boundary $z = -h$ is specified by the formulas

$$V_n = V, |x| < a, |y| < b; V_n = 0, |x| > a \text{ or } |y| > b, \quad [12]$$

where the vertical velocity of the ice beam $V = V(t)$ is a function of the time. The velocity potential was constructed in analytical form with using of Fourier transform (Grue, 2017). The mean added mass per unit area of the beam surface equals

$$\langle m_{ad} \rangle = \frac{4\rho_w b}{\pi^2} \int_0^\infty \int_0^\infty \frac{(\sin u)^2 (\sin v)^2}{uv\sqrt{(ub/a)^2+v^2}} du\, dv. \quad [13]$$

The characteristics of ice beams used in the experiments are $a_1 = 5$ m, $b_1 = 0.2$ m, $h_1 = 0.72$ m, $T_1 = -6.5$ C, $S_1 = 4.94$ ppt; $a_2 = 2.4$ m, $b_2 = 0.25$ m, $h_2 = 0.515$ m, $T_2 = -4.2$ C, $S_2 = 0.0$ ppt. The calculated added masses in the experiments are $\langle m_{ad} \rangle_1 = 0.561\rho_w$(kg/m^2) ($\rho_w = 1020$ kg/m^3) and $\langle m_{ad} \rangle_2 = 0.554\rho_w$(kg/m^2) ($\rho_w = 1000$ kg/m^3).

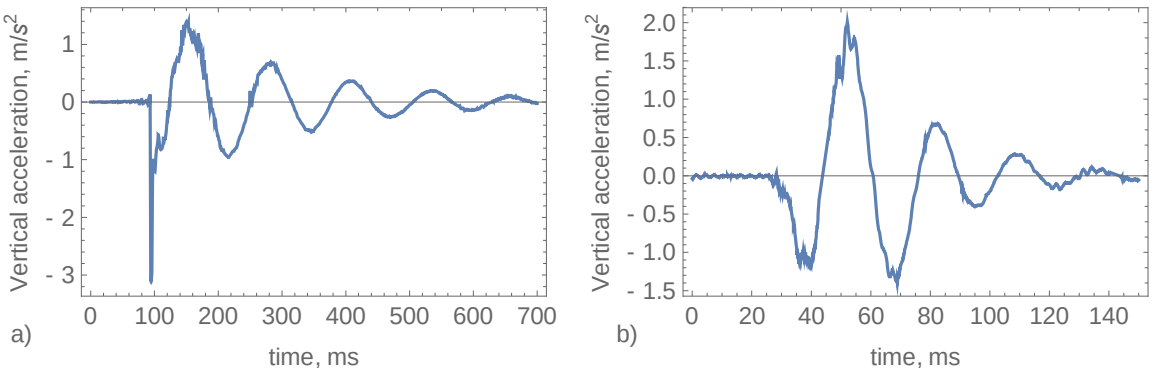

Figure 7. Examples of the vertical accelerations of the beams recorded in the test 1 in sea ice (a) and in the test 2 in lake ice (b).

Examples of the acceleration records are shown in Fig. 7. The frequencies of the beam oscillations in the test 1 and 2 are estimated as $\omega_1 \approx 16\pi$ rad/s (8 Hz) and $\omega_2 \approx 80\pi$ rad/s (40 Hz). The elastic moduli calculated with formula [11] are $E_1 = 2$ GPa annd $E_2 = 6$ GPa.

Numerical simulations in Comsol Multiphysics 5.4 were performed to calculate natural frequency of the plates on elastic foundation. The goal of numerical simulations was to account displacements of the fixed-ends beams near their roots. Boundary conditions [3] don't correspond to real situation because the ice near the beam roots may have vertical displacements excited by the beam oscillations. Numerical simulations were performed in the plate mode, where the thickness of the plate was equal to the beam thickness. The added mass was programmed as a property of the beams, while the added mass of the other parts of the plate in the computational domain were equal to zero. We adjusted the elastic modulus of the frequency of a natural mode with big amplitude of the beam and relatively small amplitudes in the rest of the computational domain to the measured frequencies by iterations. Obtained values of the elastic moduli in the test 1 and 2 are $E_{1,fe} = 2.8$ GPa and $E_{2,fe} = 11.0$ GPa.

4. Tests with vibrating cantilever beams

Two horizontal beams were made from sea ice collected in the Vallunden lake (lagoon) in the Van Mijen fjord in March 2019 and from fresh-water ice in the lake near Longyearbyen in November 2019. Their dimensions were $a_1 = 8.0$ cm, $b_1 = 7.25$ cm, $l_1 = 48$ cm and $a_2 = 7.0$ cm, $b_2 = 6.0$ cm, $l_2 = 50$ cm. In the experiments the beams temperature was -12 C. The subscripts 1 and 2 are related to sea ice beams and fresh ice beams. The beam shape is shown in Fig. 8 (right panel). Two accelerometers Bruel & Kjær DeltaTron Type 8344 are also visible in the photograph. The beam oscillations were excited by a finger. The accelerometers measured vertical accelerations directed along the axis z (left panel in Fig. 8). The optical axes of ice were perpendicular the axis z. This test is further named VCB test.

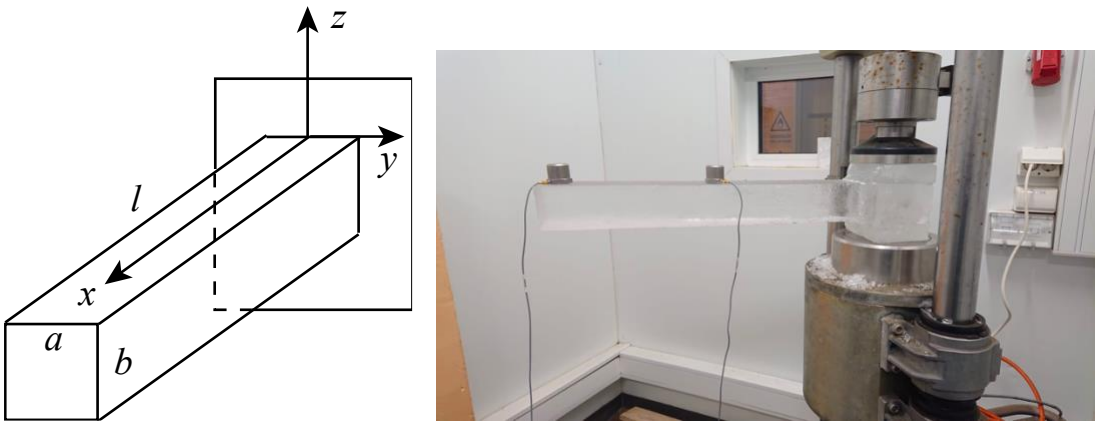

Figure 8. Schematic of the test with vibrating cantilever beam (left panel) (VCB test). Photograph of the test, the accelerometers are mounted on the top surface of the beam (right panel).

The first natural frequency of cantilever beam is calculated with formula (Landau and Lifshitz, 1965)

$$E = \frac{\omega^2 l^4}{3.52^2}\frac{\rho_i S}{I_y},\ S = ab,\ I_y = \frac{ab^3}{12}, \qquad [14]$$

where l is the beam length, and a and b are dimensions of the beam in the transversal direction to the axis (left panel in Fig. 8).

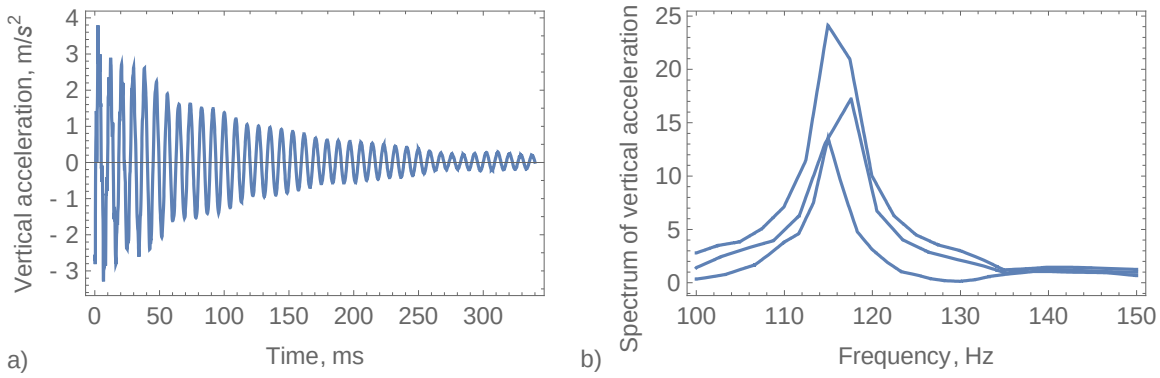

Figure 9. Example of the acceleration record (a) and spectrums of the vertical accelerations (b) in the tests with sea ice beam.

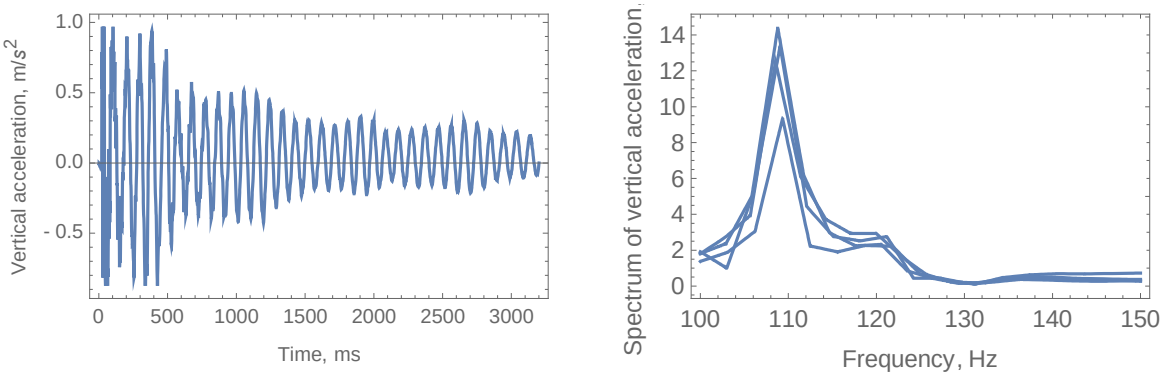

Figure 10. Example of the acceleration record (left panel) and spectrums of the vertical accelerations (right panel) in the tests with fresh ice beam.

The example of the accelerometer record in the test with sea ice and fresh ice beams are shown in the left panel of Fig. 9, and Fig.10. The right panels on the same figures show the Fourier-spectrum of the acceleration signal. The values of the frequencies in the spectral maxima were $\omega_1 = 230\,\pi$ rad/s (115 Hz) for the sea ice beam, and $\omega_2 = 218\,\pi$ rad/s (109 Hz) for the lake ice beam. The elastic moduli calculated with formula (25) were $E_1 = 4.7$ GPa and $E_2 = 7.2$ GPa respectively.

Numerical simulations in Comsol Multiphysics 5.4 were performed to calculate natural frequencies of the oscillations of the beams with the shapes similar the shapes of the beams used in the experiment. The right panel in Fig. 8 shows that the fixed ends of the beams were wider than their main body. Simulations were performed in the 3D elastic mode of the program. The elastic moduli were adjusted by the iterations approaching the measured natural frequency to the calculated natural frequency. Obtained values of the elastic moduli were $E_{1,fe} = 5.55$ GPa for the sea ice beam and $E_{2,fe} = 8.25$ GPa for the lake ice beam.

5. Acoustic measurements

Acoustic measurements were performed on March 9, 2016, in the same location (Van Mijen fjord, Vallunden lake). The air temperature was of around -4C, the surface ice temperature was -3C, and the bottom ice temperature was at the freezing point of around -1.87C. The ice thickness was 60 cm. Sea ice salinity varied from 6 ppt near the bottom to 2 ppt near the surface. The mean salinity averaged over the ice thickness was 4.38 ppt. We used a Vallen AMSY-5 to send and receive acoustic pulses with peak frequency of 150 kHz through PZT-5H compressional crystal transducers. The transducers were frozen onto the surface of an ice core taken from the naturally formed sea ice cover. Experiments were conducted within one hour of coring. Some brine drainage occurred. The core was 600mm long, covering the full vertical extent of the ice, with fragile and mushy ice removed from the bottom. The core was 140mm in diameter. The Vallen acoustic processing unit has a calibration setting which allows us to send out pulses at one transducer and then detect them at other transducers (AT test). Pulsing from transducer 1 to transducer 4, and vice versa, we found travel times of 197μs over a distance 600 mm, which corresponds to a speed of sound of 3040ms^{-1}. The elastic modulus calculated with the formula $E = \rho_i c_p^2 (1+\nu)(1-2\nu)/(1-\nu)$ is equal to 5.7 GPa when the ice density is $\rho_i = 917$ kg/m^3, the speed of p-wave is $c_p = 3040$ m/s, and the Poisson's ratio is $\nu = 0.33$.

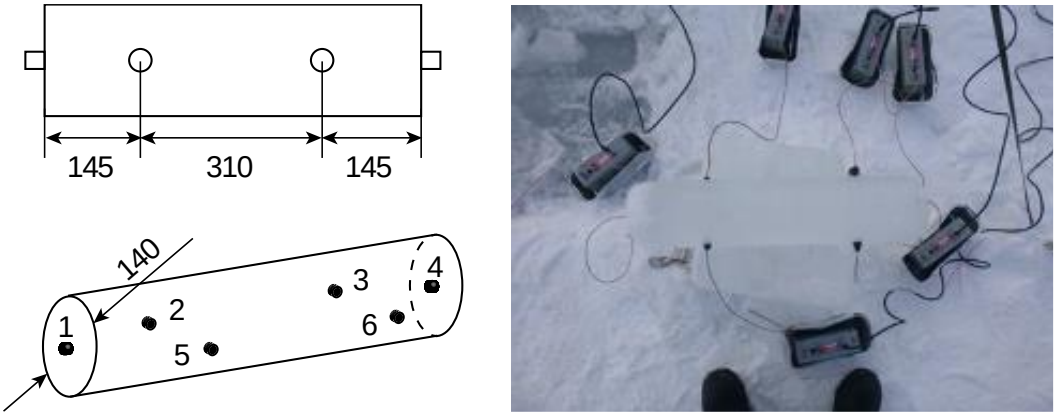

Figure 11. Dimensions of the ice core and locations of acoustic transducers in AT test (left). Photograph of the AT test on acoustic measurement of p-waves speed (right).

Any errors are most likely to occur in measurement of distance, since the measurements in time are software-controlled and highly repeatable. We tried to be careful measuring the distance between transducers 1 and 4, but the measurement could be out by as much as 20mm either way. This gives a range of $2940ms^{-1}$-$3140ms^{-1}$. Transducers 5 and 6 give results which are difficult to interpret, and we suspect they may have had loose wiring. This means we're not able to compare vertical and horizontal sound speeds in the ice.

6. Conclusions and discussion

Results of the calculation of the elastic moduli from the experimental data are shown in Fig. 1 for the tests with fresh-water ice and in Fig. 2 for the tests with sea ice. The liquid brine content is calculated according to formula of Frankenstein and Garner (1967). Most of elastic moduli of fresh ice are lower than it is predicted by Sinha's formulas (1). The value of the elastic modulus of 11 GPa obtained by the numerical simulations of the natural frequency of fixed-ends beam is higher than it is predicted by formula (1). This result can't be considered as reliable because the model of water was simplified to the elastic foundation below the main part of the computational domain, and only below the beam the water effect was accounted by the added mass. VCB tests showed higher values of the elastic modulus than FCB and VFEB tests in the experiments with sea ice and fresh ice. Higher frequencies in VCB tests in comparison with VFEB tests may explain higher elastic modulus measured in VCB test.

Frequency response of effective elastic modulus was investigated by Sinha (1978) for polycrystalline fresh ice. He explained a reduction of the elastic modulus with frequency decrease by the influence of viscous-elastic rheology. The reduction exceeded 50% when the frequency changed from 10 Hz to 0.001 Hz, i.e. in the range of very low frequencies. The redaction was less than 10% when the frequency changed from 1 MHz to 1 Hz. For fresh columnar ice we obtained the reduction of elastic modulus from 7.2 GPa in VCB tests performed with the frequency of 109 Hz, to 6 GPa in VFEB tests performed with the frequency of 40 Hz, and to 5.7 Hz in FCB tests which frequency is around 1 Hz. It means 20%-reduction when frequency changes from 109 Hz to 1 Hz. The ice temperature in VFEB and FCB tests was -4 C, and VCB test was performed with ice temperature -12 C. According to formula (1) temperature effect on elastic modulus can't explain this difference.

The frequencies of oscillations of sea ice beams in VCB tests were 115 Hz, and in VFEB tests – 8 Hz. Elastic moduli obtained from FCB and VFEB tests on sea ice are well approximated by the ISO19906 line described by formula (3). Elastic moduli obtained from VCB tests

showed higher values of the elastic modulus than it is predicted by formula (3), The ice temperature in the tests was -12 C. Therefore, the liquid brine content of ice and ice porosity in VCB tests are lower than in FCB and VFEB tests performed on sea ice with mean temperature of -6C. The elastic moduli were found similar and of around 2 GPa in FCB and VFEB tests. Acoustic measurements performed on similar ice with the frequency of 150 kHz showed the elastic modulus of 5.7 GPa. This result fits well to the measurements of Slesarenko and Frolov (1972) performed by ultrasonic method. Seismic measurements performed in March 2019 in the same place (Vallunden lake, Van Mijen fjord) in the frequency range of 1-200 Hz show the elastic modulus of 4.5 GPa (Moreau et al, 2020). The frequency dependence of elastic modulus of sea ice seems very significant: it increases from 2 GPa to 5.7 GPa when the frequency increases from 1 Hz to 150 kHz.

Strong damping of beams oscillations was observed in VCB and VFEB tests both. In VFEB tests damping in the test with fresh ice was stronger than in the test with sea ice, and the frequency of beam oscillations in the tests with fresh ice (40 Hz) was higher in 5 times than in the test with sea ice (8 Hz). The source of the damping can be related to the viscous processes in ice, with vorticity production in the water, and with water-ice friction. The damping time was about 5 periods of the beam oscillations in the tests. Damping of the beam oscillations in VCB tests was smaller, and the damping time is estimated about 40 periods of the beam oscillations. Damping is these tests is related mainly to viscous properties of ice, but the interaction of the beam with the air also could be important over relatively long time. Further estimates should be performed to quantify physical nature of the damping observed in the tests.

Acknowledgments
The work was supported by the Research Council of Norway through the IntPart project Arctic Offshore and Coastal Engineering in Changing Climate and Petromaks-2 project Dynamics of Floating Ice.

References

Assur, A., 1971. Forces in moving ice fields. POAC-1971, 1, 112-118.

Bogorodskii, V.V., 1964. Elastic moduli of ice crystals. Soviet Physics Acoustics, 10, 124-126.

Dantl, G., 1969. Elastic moduli of ice. Physics of Ice, Editors Riehl, N., Builemer, B., and Engelhardt, H., Plenum Press, New York, 223-230.

Frankenstein, G.E., Garner, R., 1967. Equations for determining the brine volume of sea ice from 0.5 to 22.9oC. J. Glaciology, 6(48), 943-944.

Green, R.E., Mackinnon, L., 1956. Determination of the elastic constants of ice single crystals by an ultrasonic pulse method. The Journal of the Acoustic Society of America, 28(6), 1292.

Iona, F., Scherrer, F., 1952. Die elastischen Konstanten von Eis-Einkristallen. Helv. Phys. Acta, 25, 35-54.

Grue, J., 2017. Ship generated mini-tsunami. J. Fluid Mech., 816, 142-166.

Karulin, E., Marchenko, A., Sakharov, A., Karulina, M., Chistyakov, P., Onishchenko, D., 2019. Features of determining the ice flexural strength and the elastic modulus based on floating cantilever beam tests. POAC-12.

Karulina, M., Marchenko, A., Karulin, E., Sodhi, D., Sakharov, A., Chitsyakov, P., 2019. Full-scale flexural strength of sea ice and freshwater ice in Spitsbergen Fjords and North-West Barents Sea. Applied Ocean Research. 90, 101853.

Landau, L.D., Lifshitz, E.M., 1970. Theory of Elasticity (Volume 7 of A Course of Theoretical Physics). Pergamon Press.

Langleben, M.,P., Pounder, E.,R., 1963. Elastic parameters of sea ice. In: W.D.Kingery (Editor), Ice and Snow, M.I.T. Press, Cambridge, Mass, 69-78.

Sinha, N., 1978. Short-term rheology of polycrystalline ice. J. Glaciology, 21(85), 457-472.

Sinha, N., 1989. Elasticity of natural types of Polycrystalline ice. CRST, 17, 127-135.

Ludovic Moreau, Agathe Serripierri, Pierre Boué, Jérôme Weis, 2020. Monitoring sea ice thickness and mechanical properties with seismic noise, in Proc of the Forum Acusticum, Lyon, April 2020

Slesarenko, Yu, E., Frolov, A.D., 1972. Comparison of elasticity and strength characteristics of sal-water ice. Proc. of the IAHR Symp. on Ice, 2, 85-87.

Vaundrey, K., 1977. Ice engineering – study of related properties of floating sea ice sheets and summary of elastic and viscoelastic analysis. U.S. Naval Civil Engineering Lab., Rep. TR860, Port Huenem, CA.

Voight, W., 1910. Lehrbuch Der Krystallphysik. Feubner, Berlin.

Zarembovitch, A., Kahane, A., 1964. Determination des vitesses de propagation d'ondes ultrasoneres longitudinales dans la glace, Academic Science, Paris, 2629-2532.